Unexpected Physical Phenomena Indicated by FDTD Modeling of the Sigma-60 Deep Hyperthermia Applicator

Christopher E. Reuter, *Member, IEEE*, Allen Taflove, *Fellow, IEEE*, Vythialingam Sathiaseelan, Melinda Piket-May, *Member, IEEE*, and Bharat B. Mittal

***Abstract*— We investigate the numerical convergence properties of two-dimensional (2-D) and three-dimensional (3-D) finite-difference time-domain (FDTD) models of the BSD-2000 Sigma-60 annular phased array used for deep hyperthermia. The FDTD modeling data indicate unexpected physical phenomena for the case of Sigma-60 excitation of an elliptical tissue phantom embedded in a circular water bolus. These phenomena include: 1) high-Q energy storage; 2) electromagnetic (EM) mode flipping within the water bolus/phantom; and 3) whispering-gallery transmission of energy to the opposite side of the phantom relative to the exciting dipole pair. We conclude that these phenomena substantially impact the FDTD numerical modeling of this system, and further conclude that the whispering-gallery effect can impact clinical applications of the Sigma-60.**

***Index Terms*— Electromagnetic fields, FDTD, hyperthermia, modeling.**

I. Introduction

SUBSTANTIAL literature has arisen regarding electromagnetic (EM) hyperthermia, i.e., the application of EM energy of various frequencies to heat cancerous tumors. Examples include: 1) superficial waveguide applicators for surface tumors [1]; 2) interstitial probes to heat tumors accessible via catheter [1], [2]; and c3) annular phased-array (APA) applicators used to heat deep tumors [2]. An example of a commercially available EM deep hyperthermia unit is the BSD-2000 with the Sigma-60 APA, shown schematically in Fig. 1. This system has four RF amplifiers, each driving a pair of 44-cm-long flared dipole antennas radiating in the frequency range of 60–120 MHz. The eight dipole antennas are equally spaced around a 60-cm-diameter clear plastic annulus, and are phased to provide constructive interference of the energy deep inside the body of a patient centered in the annulus. Energy is coupled from the antennas to the patient via a water bolus filling the space between the plastic annulus and the patient.

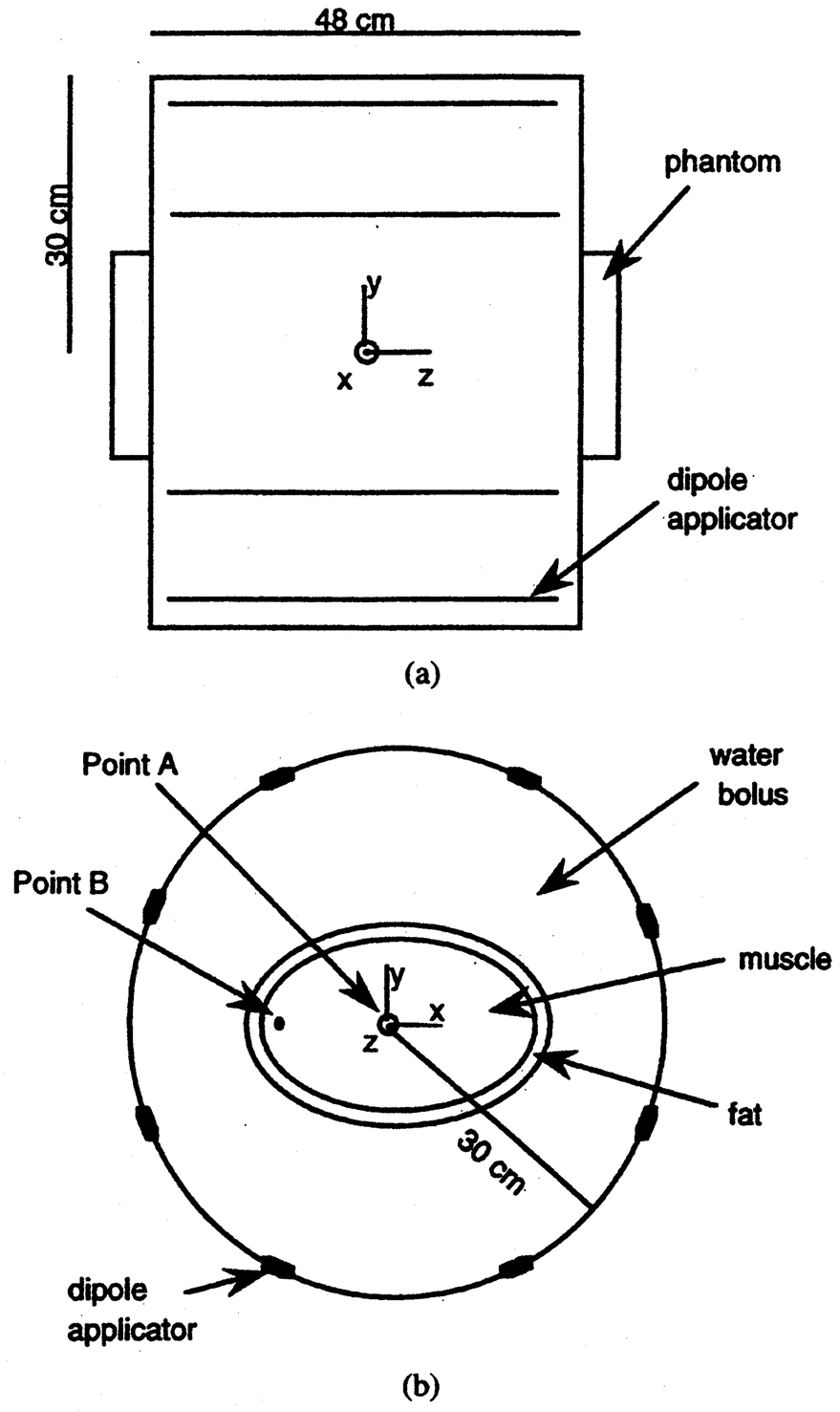

Fig. 1. Schematic representation of the BSD-2000 Sigma-60 applicator and the CDRH phantom. The eight dipole applicators are equally spaced around a 60-cm clear plastic annulus. The phantom has a 1-cm-thick rigid fat-equivalent shell surrounding a muscle-equivalent gel. (a) Longitudinal view. (b) Transverse cross section at $z = 0$.

The primary difficulty in clinical application of the Sigma-60 APA is a lack of detailed understanding of energy deposition patterns. This limits strategies to concentrate energy deposition in specific regions deep within the body. Measurements of electric fields and specific absorption rate (SAR) inside phantom models have been used to simulate patient treatments [3], [4].

This paper discusses finite-difference time-domain (FDTD) simulations [5], [6] of the excitation of a human-tissue phantom by the BSD-2000 with the Sigma-60 APA. There exists

Manuscript received November 12, 1993; revised January 14, 1998. This work was supported in part by the American Cancer Society, Illinois Division, under Grant 90-52.

C. E. Reuter is with the U.S. Air Force Research Laboratory, Rome Research Site, Rome, NY 13441-4505 USA.

A. Taflove is with the Department of Electrical and Computer Engineering, Northwestern University, Evanston, IL 60208-3118 USA.

V. Sathiaseelan and B. B. Mittal are with the Radiation Oncology Department, Northwestern Memorial Hospital, Chicago, IL 60611 USA.

M. Piket-May is with the Department of Electrical and Computer Engineering, University of Colorado, Boulder, CO 80302 USA.

Publisher Item Identifier S 0018-9480(98)02725-2.

a number of papers involving FDTD simulation of EM-wave interactions with biological systems and RF and microwave hyperthermia for cancer treatment; early examples include [7]–[15]. In this paper, we describe specific unexpected physical phenomena for the Sigma-60 APA revealed by our FDTD modeling. These phenomena include delayed convergence to the sinusoidal steady state due to high-Q energy storage, EM-mode flipping, and the whispering-gallery effect. We also describe an experimental validation obtained in the hyperthermia facility at Northwestern Memorial Hospital. We conclude that the physical factors discussed in this paper should be accounted in future FDTD simulations of structures similar to the Sigma-60 APA, and perhaps more importantly, one of these factors (the whispering-gallery effect) should be accounted in clinical applications to prevent unwanted heating of healthy tissues far from the excited dipoles.

II. FDTD Models of the CDRH Phantom

Our simulations involved a phantom developed by the Center for Devices and Radiological Health (CDRH) of the U.S. FDA [3]. Fig. 1(b) shows the position of the phantom relative to the Sigma-60 antenna-array elements at the mid-plane ($z = 0$) of the array in Fig. 1(a). This cross section is designated the x–y plane. The phantom is a 57-cm-long elliptical inhomogeneous dielectric cylinder with major and minor axes of 32 and 22 cm, respectively. A 1-cm-thick rigid epoxy shell with the electrical properties of fat ($\varepsilon_r = 10, \sigma = 0.01$ S/m) encloses a gel material having the electrical properties of muscle ($\varepsilon_r = 65, \sigma = 0.90$ S/m) at the frequency of interest [16].

The two-dimensional (2-D) FDTD model assumes that there is no change of either geometry or excitation in the z-direction from that depicted in Fig. 1(b). The Sigma-60 APA is positioned about the center of the grid, Point A (0, 0). All grid cells within a 30-cm-radius circle centered at (0, 0) are assigned the electrical properties of water, fat, or muscle as appropriate to the phantom and water-bolus geometry shown in Fig. 1(b). All remaining grid cells are assigned the properties of air except for eight points that are assigned the properties of metal to represent the dipoles of the Sigma-60.

The three-dimensional (3-D) FDTD model incorporates all significant parts of the Sigma-60 and CDRH phantom, as shown in Fig. 1(a) and (b). The eight exciting dipoles are modeled as thin wires excited at the center gap with a sinusoidal electric-field source. A grid resolution of 1 cm is used. As a result, the Sigma-60 with phantom spans a grid volume of 60 × 60 × 58 cells in the x-, y-, and z-directions, respectively.

Our work focuses on FDTD modeling of two treatment protocols at 110 MHz for which we have generated experimental phantom data. For the first experimental case, the Sigma-60 heats an imaginary tumor centered at coordinates (0, 0, 0). To model this central-heating case using FDTD, we simulate equal-magnitude and zero-phase 110-MHz sinusoidal excitation applied to all applicators. This is in accord with the protocol assigned by the BSD-2000 software when constructive interference is desired at the center of the APA. In the second experimental case, the Sigma-60 heats only one side of the phantom. Power is applied only to the left pair of dipoles while the remaining antennas are permitted to float in an unexcited manner. All numerical calculations were performed on a single processor of the CRAY Y-MP. Typical runs took approximately 400 s for the 2-D model and 6000 s for the 3-D model.

In the course of our computational and experimental investigations, we observed three interesting physical phenomena not previously reported. We discuss these results in the following sections.

III. Delayed Convergence Due to High Q

A major concern when applying the FDTD method is the computer time required to compute the desired fields. One factor affecting the computation time is the Q (ratio of stored to dissipated energy) of the system. High-Q systems require prolonged time stepping to reach the desired sinusoidal steady state or late-time impulse response, or the use of linear prediction or similar means to extrapolate a narrowly time-windowed impulse response [17].

The literature indicates that the sinusoidal steady state is reached within 2–6 RF cycles (sinusoidal periods) of the exciting field for a broad range of FDTD models of the interaction of EM waves with biological tissues [7]–[15]. However, in this work involving the Sigma-60 APA, comparison of the computed electric-field (E-field) amplitude distribution in the phantom during RF cycles 1–15 reveals that no two successive distributions are similar. This implies that the sinusoidal steady state is not reached within the first 15 RF cycles. In fact, at 110 MHz, the 2-D FDTD model requires more than 100 RF cycles to converge.

Investigation of the physical convergence of the model requires monitoring the change of the computed E-field amplitude at several locations in the phantom during progressive time-stepping. Two of these observation points in the 2-D model are designated A and B in Fig. 1(b), located at coordinates (0, 0) and (−15 cm, 0), respectively. These points represent the observed extremes of the convergence properties of the FDTD model at 110 MHz. That is, the E-field amplitude at Point A converges in the minimum number of computed RF cycles, while the E-field amplitude at Point B converges in the maximum number of RF cycles. All other locations within the phantom converge after Point A or before Point B.

Fig. 2 illustrates the results of the convergence studies for 110-MHz excitation of the 2-D model at Points A and B. From this figure, we see that the computed E-field amplitude at centrally located Point A reached the sinusoidal steady state within about the first ten RF cycles. However, the computed E-field amplitude at Point B near the edge of the phantom has large oscillations extending over hundreds of RF cycles. It is clear that data obtained for Point B before RF cycle 200 is not even close to the sinusoidal steady state.

Fig. 3(a) and (b) illustrates, respectively, the E-field amplitude responses at Points A and B for sinusoidal excitations at 10-MHz increments in the range 70–120 MHz. As seen in Fig. 3(a), centrally located Point A reaches the sinusoidal

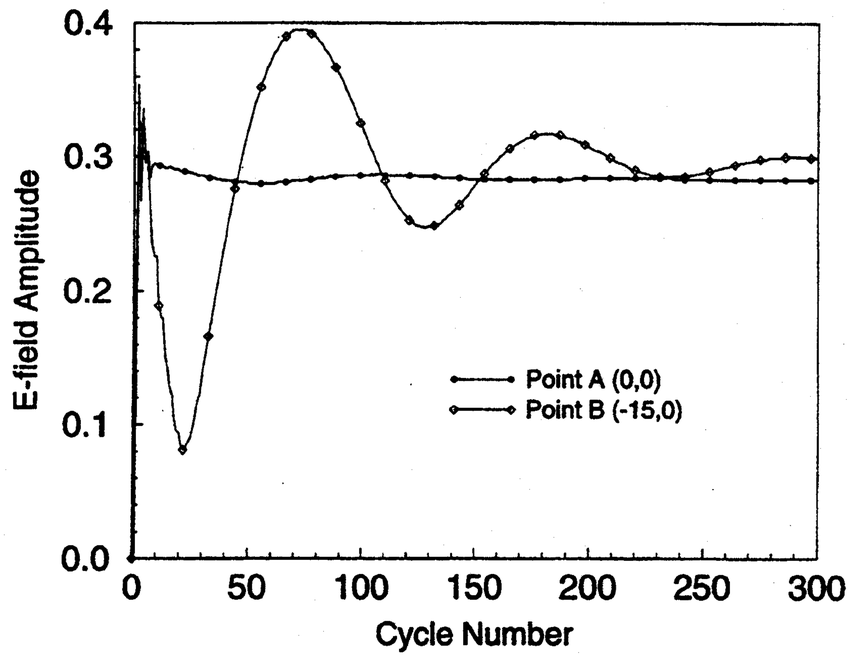

Fig. 2. Electric-field amplitude versus RF cycle number for the 2-D FDTD model at observation Point A (0, 0) and Point B (−15 cm, 0) of Fig. 1(b) within the phantom for the case of 110-MHz equal-magnitude and zero-phase excitation of the annular phased array.

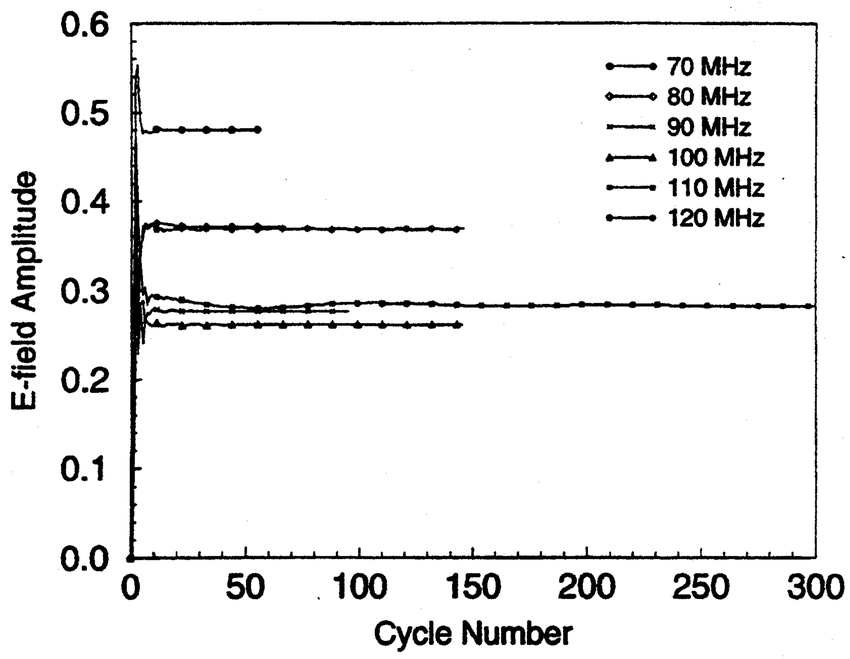

(a)

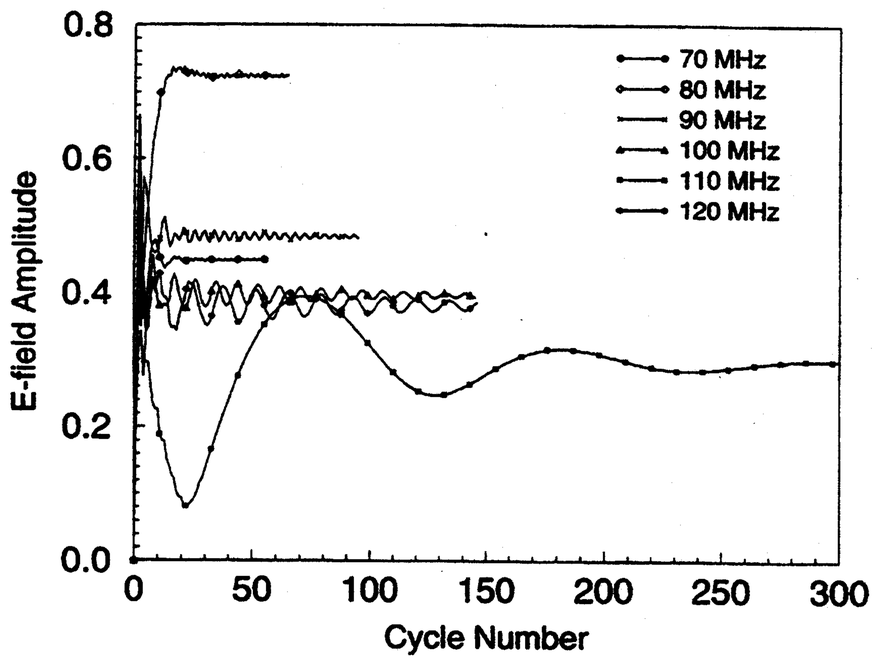

(b)

Fig. 3. Electric-field amplitude versus RF cycle number for the 2-D FDTD model of Fig. 1(b) for 70-, 80-, 90-, 100-, 110-, and 120-MHz equal-magnitude and zero-phase excitation of the annular phased array. (a) Observation Point A. (b) Observation Point B, showing pronounced oscillatory behavior at 110 MHz.

steady state within about 10 RF cycles for all of these frequencies. However, Fig. 3(b) shows that peripherally located Point B exhibits varying degrees of delayed convergence. The slowest convergence for Point B is at 110 MHz, where a pronounced oscillatory behavior is observed. Further, perturbing the frequency by only ±10 MHz results in a substantial reduction of this oscillatory behavior. This indicates a type of resonance at 110 MHz for the 2-D model.

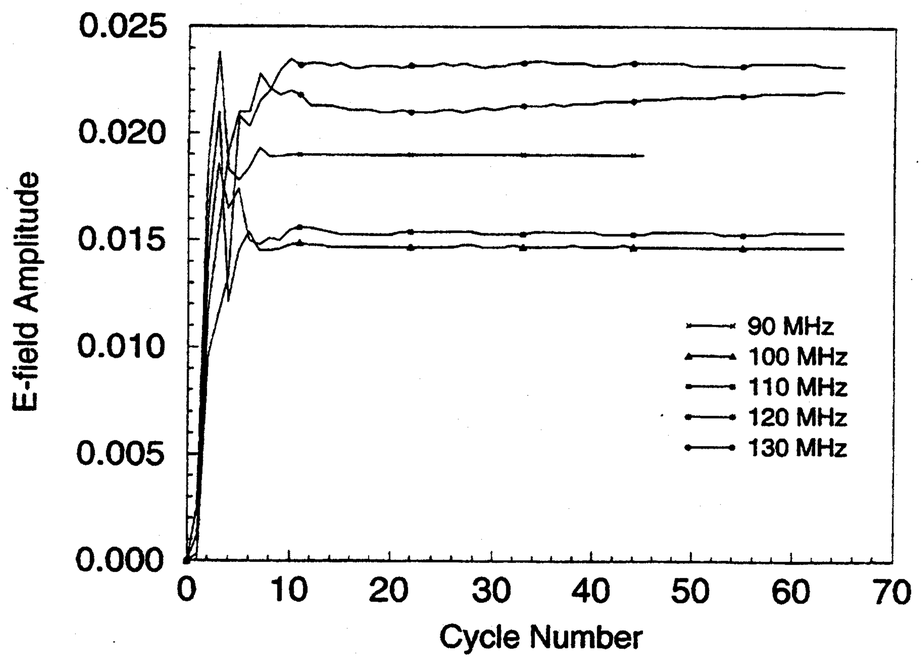

(a)

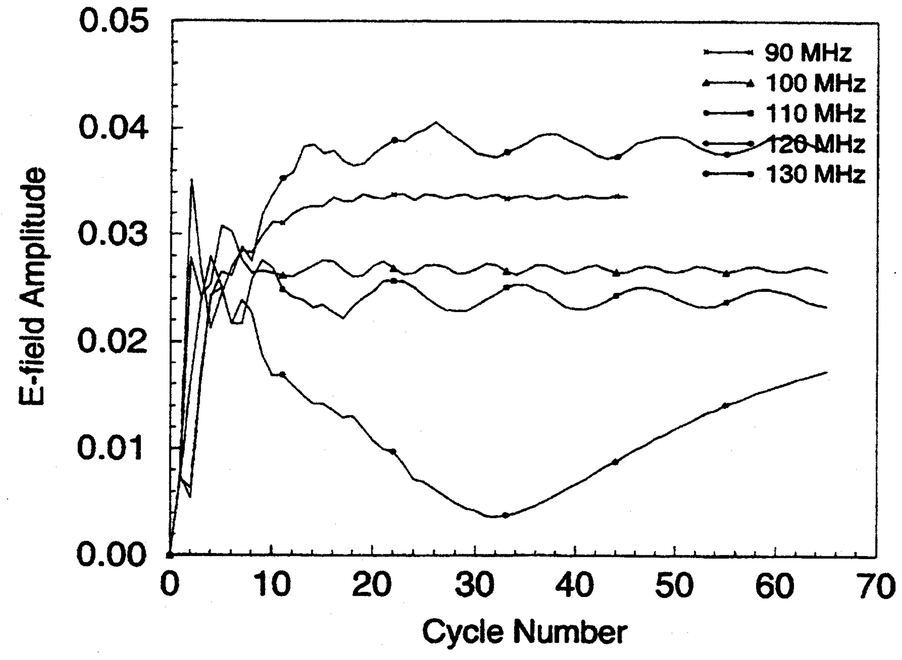

(b)

Fig. 4. Electric-field amplitude versus RF cycle number for the 3-D FDTD model for 90-, 100-, 110-, 120-, and 130-MHz equal-magnitude and zero-phase excitation of the annular phased array. (a) Observation Point A (0, 0, 0). (b) Observation Point B (−15 cm, 0, 0), showing pronounced oscillatory behavior at 120 MHz.

We have observed similar results for excitations between 90–130 MHz in 3-D models of the Sigma-60. Fig. 4(a) and (b) shows the computed results for the E-field amplitude at the two observation points in the phantom corresponding to Points A and B discussed above, but located in the middle x–y plane ($z = 0$) of the model. In Fig. 4(a), centrally located Point A reaches the steady state within the first 15 RF cycles for all frequencies shown. However, in Fig. 4(b), the E-field amplitude at peripherally located Point B oscillates in a manner similar to the 2-D results shown in Fig. 3(b). Whereas the 2-D results indicate a resonance around 110 MHz, the 3-D results indicate that the resonance is shifted to approximately 120 MHz. At this frequency, the largest oscillation and slowest convergence at the periphery of the phantom is noted. Again, a shift of only ±10 MHz shows greatly reduced amplitude oscillations at Point B. At the worst case (120 MHz), more than 100 RF cycles must be time stepped to reach an approximate steady state at all points. For the 110-MHz studies of this paper, time stepping through approximately 60 RF cycles is sufficient for convergence.

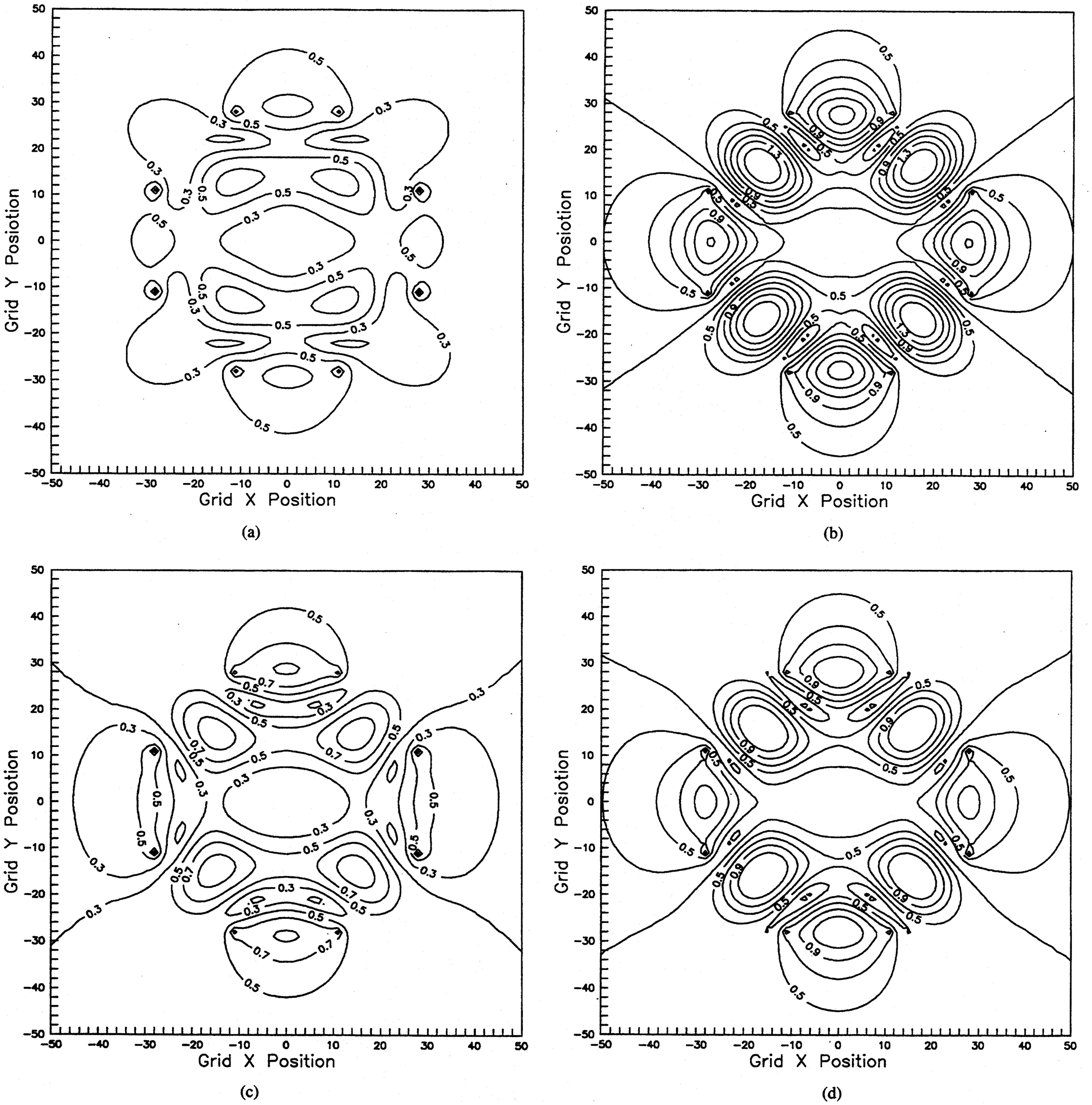

Fig. 5. Distinct modal patterns of the E-field observed within the phantom and water bolus of the 2-D model for 110-MHz equal-magnitude and zero-phase excitation of the annular phased array. (a) After 5 RF cycles, (b) 45 cycles, (c) 85 cycles, and (d) 125 cycles.

IV. Mode Flipping Near Resonance

Another unexpected effect—"mode flipping"—is observed to occur near the 110- and 120-MHz resonances of the 2-D and 3-D FDTD models for the central-heating configuration during the early sinusoidal cycles before convergence. This is revealed by constructing a contour map of the spatial distribution of the E-field within the phantom and water-bolus structure at the completion of each RF cycle of time stepping. We observe that this spatial distribution alternates between two completely different modes before ultimate convergence to the sinusoidal steady state.

Fig. 5 shows the two distinct modal patterns observed for the 2-D model. Here, the E_z-field distribution within the phantom/bolus is plotted after 5 RF cycles [Fig. 5(a)], 45 cycles [Fig. 5(b)], 85 cycles [Fig. 5(c)], and 125 cycles [Fig. 5(d)]. A color video of these data indicates a pronounced hysteresis-like effect wherein the modal pattern appears stable over many RF cycles, but then quickly flips to the opposite state over just a few cycles. Additional analysis reveals that this mode flipping is periodic with one complete repetition each (approximately) 80 RF cycles. 3-D computations indicate similar mode flipping. However, because of the large computer

time needed to time-step through the hundreds of RF cycles required to discern the oscillations of the modal pattern at 120 MHz (see Fig. 4(b), 120-MHz data) we report only the 2-D mode-flipping results.

V. Whispering-Gallery Effect Near Resonance

The final unexpected phenomenon reported here is a "whispering-gallery" effect that occurs when only a single dipole pair of the Sigma-60 is excited. Excitation of a single dipole pair should heat only the side of the phantom immediately adjacent to that pair. However, apparently due to geometrical reflection effects within the circular water bolus, both the 2-D and 3-D FDTD models show that significant EM energy is coupled to the opposite side of the phantom relative to the exciting dipole pair. These results are so intriguing that additional physical experiments probing the phenomenon have been performed at the Northwestern Memorial Hospital Hyperthermia Facility.

A. Details of the Physical Experiment and Its Simulation

We now describe the experimental validation of the FDTD predictions of the whispering-gallery effect. The experiment uses a specialized phantom employing a grid of light-emitting diodes (LED's) [4]. This LED grid is placed into a saline phantom to directly visualize the applied E-field pattern produced by the BSD Sigma-60. In addition to qualitatively mapping the distribution of the penetrating E field, quantitative data for this field are obtained by calibrating the turn-on potential for the LED's.

The LED phantom is an 82-cm-long hollow cylinder of elliptical cross section having major and minor axes of 36 and 24 cm. The curved cylinder wall is made of 2-mm-thick red polyvinyl chloride (PVC), and the two end walls are made of clear PVC. Thus, the LED's contained within the interior of the cylinder can be directly viewed and photographed through the end walls. The phantom is filled with 3 g/L saline (NaCl) solution to approximate the volume-averaged electrical properties of human tissue at frequencies near 100 MHz ($\varepsilon_r = 77, \sigma = 0.55$ S/m) [4]. A 3-mm-thick Plexiglas (acrylate) plate of elliptical shape slightly smaller than the phantom's cross section forms a grid for 143 LED's spaced at 2-cm intervals, which is placed at the midplane ($z = 0$) of the saline phantom. Each LED has its leads bent to form a 4.7-cm-long dipole which is oriented perpendicular to the plane of the grid to detect the dominant E-field component.

An important feature of the FDTD model of the LED phantom is its detailed simulation of all 143 LED's and associated dipoles. The literature indicates that the presence of these sensing devices significantly perturbs the ambient E-field distribution [4]. This perturbation must be accounted in any valid model. In the present FDTD simulation, each LED sensing device is modeled as a pair of thin 2.0-cm-long wires loaded by a lumped resistor-capacitor equivalent circuit for the LED [19]. As measured in our laboratory, the LED equivalent circuit at 110 MHz consists of the parallel combination of a 90-Ω resistor and a 48.2-pF capacitor. No LED nonlinearity is modeled. Adjacent sensing dipoles/LED's are spaced at 2-cm intervals in a planar rectangular matrix.

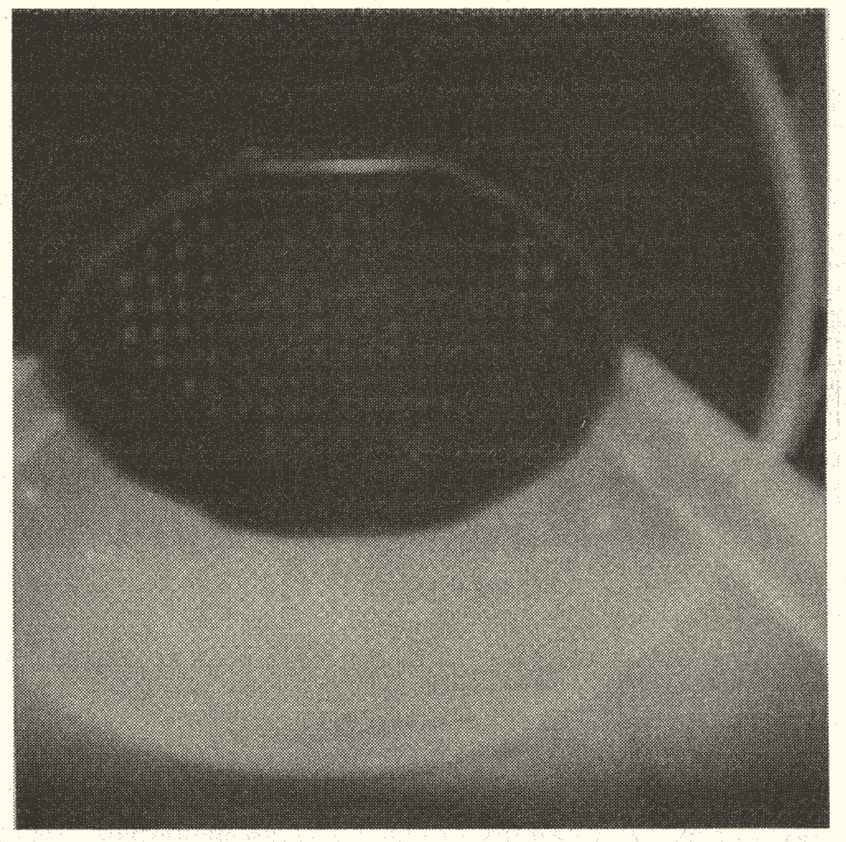

Fig. 6. Photograph of the LED sensing matrix in the midplane of the phantom with 235 W of 110-MHz RF power applied to only the left pair of Sigma-60 applicator dipoles. Note the excitation of several LED's at the right (opposite) side of the phantom.

An additional feature of the FDTD model of the LED phantom (relative to earlier models of the CDRH phantom) is that the dielectric geometry accounts for the sagging of the water bolus under the force of gravity. This sagging causes a significant up–down geometrical asymmetry.

The simulated RF power P applied to each of the two left applicator dipoles of the Sigma-60 in the FDTD model is calculated by $P = VI\cos\theta$. Here, the terminal voltage V, terminal current I, and relative phase θ are obtained at the applicator–dipole center gap by implementing a Faraday's Law contour integral of the E-field across the gap and an Ampere's Law contour integral of the H-field curling around the gap [18]. The E-field in the simulated Sigma-60 applicator dipole gap is scaled to achieve a power level of 117.5 W, or a total of 235 W for the pair of applicator dipoles. This simulated RF power is equivalent to that of the physical experiment conducted at Northwestern Memorial Hospital.

B. Results

Fig. 6 is a photograph of the embedded LED matrix under conditions of 235 W applied to the left pair of Sigma-60 applicator dipoles. This figure clearly shows that there is LED turn-on within the sensing matrix at the right (opposite) side of the phantom farthest away from the excited pair of applicator dipoles.

Fig. 7 depicts the corresponding FDTD predictions for the axial (z-directed) E-field component in the plane of the LED matrix. Contours of equal E-field magnitude are plotted around the LED locations. These contours are thresholded so that the only ones shown are those that surround LED's having predicted terminal voltages exceeding 1.2-V zero-to-peak, the measured potential for light emission at 110 MHz. In this figure, increasing density of the contours denotes greater LED terminal voltage and thus greater light-emission intensity. Thus, Fig. 7 visualizes the FDTD prediction of both the positions and the emitted light intensities of the lit LED's within the phantom during RF excitation.

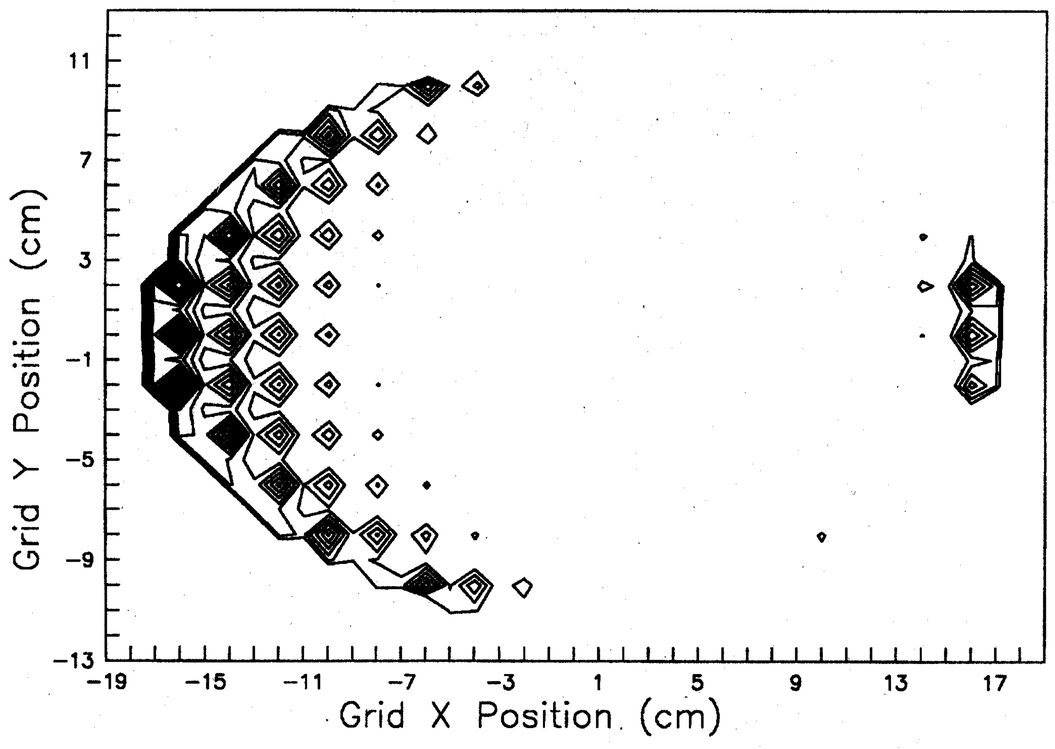

Fig. 7. FDTD predictions for the E-field at the LED sensing matrix under the conditions of Fig. 6. Contours of equal E-field magnitude are shown for LED's having predicted terminal voltages exceeding 1.2-V zero-to-peak. This provides a visualization of both the position and emission intensity of the lit LED's within the phantom, and can be directly compared to Fig. 6.

Comparing Figs. 6 and 7, we see good agreement between the FDTD model and the experimental results for light emission from the LED sensing matrix. The only discrepancy is on the right side of the phantom where the FDTD model somewhat underestimates the number of lit LED's. We view these results as a significant qualitative and quantitative experimental validation of the overall FDTD simulation and, more precisely, its prediction of a whispering-gallery effect.

VI. Discussion and Conclusions

We reported 2-D and 3-D FDTD models of the BSD-2000 Sigma-60 annular-phased-array hyperthermia device. The results indicate that previous published data for FDTD simulations of the Sigma-60 are probably not converged. Near resonance, convergence to the sinusoidal steady state for the elliptical phantom geometry requires literally hundreds of RF cycles to be time-stepped. Away from resonance, the required number of RF cycles diminishes rapidly, but is still well in excess of previously reported values.

In the course of the FDTD modeling, data have been obtained indicating additional unexpected physical phenomena. For the case of Sigma-60 excitation of an elliptical phantom embedded in a circular water bolus, these phenomena include mode-flipping and a whispering-gallery effect that causes heating on the far side of the phantom opposite to that of the excited dipole pair. An experimental validation of the whispering-gallery effect was presented. We believe that these physical phenomena can affect both the FDTD numerical modeling and the clinical applications of the Sigma-60 APA. Further critical evaluation of these issues is recommended.

Acknowledgment

The authors wish to thank Cray Research, Inc., Eagan, MN, for providing the computational resources for this work, and J. Chang and M. Greenley for their help with the LED threshold measurements.

References

[1] C. A. Perez and B. N. Emami, "Clinical trials with local (external and interstitial) irradiation and hyperthermia. Current and future perspectives," *Radiologic Clinics North America*, vol. 27, pp. 525–542, 1989.
[2] J. W. Hand and J. R. James, Eds., *Physical Techniques in Clinical Hyperthermia*. Letchworth, U.K.: Res. Studies Press, 1986.
[3] S. Allen, G. Kantor, H. Bassen, and P. Ruggera, "CDRH RF phantom for hyperthermia systems evaluations," *Int. J. Hyperthermia*, vol. 4, pp. 17–23, 1988.
[4] C. Schneider and J. D. P. Van Dijk, "Visualization by a matrix of light-emitting diodes of interference effects from a radiative four-applicator hyperthermia system," *Int. J. Hyperthermia*, vol. 7, pp. 355–366, 1991.
[5] K. S. Yee, "Numerical solution of initial boundary value problems involving Maxwell's equations in isotropic media," *IEEE Trans. Antennas Propagat.*, vol. AP-14, pp. 302–307, May 1966.
[6] A. Taflove, *Computational Electrodynamics: The Finite-Difference Time-Domain Method*. Norwood, MA: Artech House, 1995.
[7] A. Taflove and M. E. Brodwin, "Computation of the electromagnetic fields and induced temperatures within a model of the microwave-irradiated human eye," *IEEE Trans. Microwave Theory Tech.*, vol. MTT-23, pp. 888–896, Nov. 1975.
[8] R. W. Lau, R. J. Sheppard, G. Howard, and N. M. Bleehen, "The modeling of biological systems in three dimensions using the time-domain finite-difference method: I. The implementation of the model; II. The application and experimental evaluation of the method in hyperthermia applicator design," *Phys. Med. Biol.*, vol. 31, pp. 1247–1266, 1986.
[9] D. T. Borup, D. M. Sullivan, and O. P. Gandhi, "Comparison of the FFT conjugate gradient method and the finite-difference time-domain method for the absorption problem," *IEEE Trans. Microwave Theory. Tech.*, vol. MTT-35, pp. 383–395, Apr. 1987.
[10] D. M. Sullivan, D. T. Borup, and O. P. Gandhi, "Use of the finite-difference time-domain method in calculating EM absorption in human tissues," *IEEE Trans. Biomed. Eng.*, vol. BME-34, pp. 148–157, Feb. 1987.
[11] D. M. Sullivan, O. P. Gandhi, and A. Taflove, "Use of the finite-difference time-domain method in calculating EM absorption in man models," *IEEE Trans. Biomed. Eng.*, vol. 35, pp. 179–186, Mar. 1988.
[12] C. Wang and O. P. Gandhi, "Numerical simulation of annular phased arrays for anatomically based models using the FDTD method," *IEEE Trans. Microwave Theory Tech.*, vol. 37, pp. 118–126, Jan. 1989.
[13] D. Sullivan, "Three-dimensional computer simulation in deep regional hyperthermia using the finite-difference time-domain method," *IEEE Trans. Microwave Theory Tech.*, vol. 38, pp. 204–211, Feb. 1990.
[14] ———, "Mathematical methods for treatment planning in deep regional hyperthermia," *IEEE Trans. Microwave Theory Tech.*, vol. 39, pp. 864–872, May 1991.
[15] M. J. Piket-May, A. Taflove, W. C. Lin, D. S. Katz, V. Sathiaseelan, and B. B. Mittal, "Initial results for automated computational modeling of patient-specific electromagnetic hyperthermia," *IEEE Trans. Biomed. Eng.*, vol. 39, pp. 226–237, Mar. 1992.
[16] M. Stuchly and S. Stuchly, "Dielectric properties of biological substances—tabulated," *J. Microwave Power*, vol. 15, pp. 19–26, 1980.
[17] W. L. Ko and R. Mittra, "A combination of FDTD and Prony's methods for analyzing microwave integrated circuits," *IEEE Trans. Microwave Theory Tech.*, vol. 39, pp. 2176–2181, Dec. 1991.
[18] M. J. Piket-May, A. Taflove, and J. Baron, "FDTD modeling of digital signal propagation in 3-D circuits with passive and active loads," *IEEE Trans. Microwave Theory Tech.*, vol. 42, pp. 1514–1523, Aug. 1994.

Christopher E. Reuter (S'83–M'85) received the B.S. and M.S. degrees from Marquette University, Milwaukee, WI, in 1986 and 1988, respectively, and the Ph.D. degree from Northwestern University, Evanston, IL, in 1993.

Since 1994, he has been with the U.S. Air Force Research Laboratory, Rome Research Site, Rome, NY. He is currently an Electronics Engineer, where his research focuses on numerical modeling of EM phenomena. His research interests include EM effects associated with advanced electronics modules and systems involving interconnect characterization, electronics packaging and MCM problems, and EM interaction issues associated with biomedical problems.

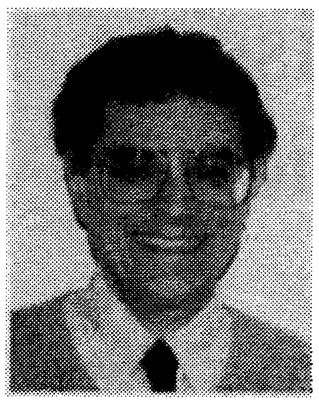

Allen Taflove (M'75–SM'84–F'90) was born in Chicago, IL, on June 14, 1949. He received the B.S., M.S., and Ph.D. degrees in electrical engineering from Northwestern University, Evanston, IL, in 1971, 1972, and 1975, respectively.

After nine years as a Research Engineer at IIT Research Institute, Chicago, IL, he returned to Northwestern in 1984, and since 1988, has been a Professor in the Department of Electrical and Computer Engineering. Since 1990, he has given many invited talks and lectures in the U.S. and abroad on FDTD and horizons in computational electromagnetics. He authored *Computational Electrodynamics: The Finite-Difference Time-Domain Method*, (Norwood, MA: Artech House, 1995) and is currently completing the editing of *Advances in Computational Electrodynamics*, (Norwood, MA: Artech House) scheduled to be published in 1998. His current research interests include FDTD simulations of VLSI-scale optoelectronic devices, pulsed confocal microwave technology for detection of early-stage breast cancers, and diffraction of cellular radio waves by the corners and rooftops of realistic buildings.

Prof. Taflove is a member of IEEE COMAR, Eta Kappa Nu, Tau Beta Pi, Sigma Xi, International Union of Radio Science (Commissions B, D, and K), and the Electromagnetics Academy. He was a Distinguished National Lecturer for the IEEE Antennas and Propagation Society (1990–1991), and Chairman of the Technical Program of the IEEE Antennas and Propagation Society International Symposium in Chicago, IL (1992). His biographical listings include *Who's Who in Engineering*, *Who's Who in America*, *Who's Who in Science and Engineering*, and *Who's Who in American Education*.

Melinda Piket-May (S'89–M'92) received the B.S. degree in electrical and computer engineering from the University of Illinois at Urbana-Champaign, in 1988, and the M.S. and Ph.D. degrees in electrical and computer engineering from Northwestern University, Evanston, IL, in 1990 and 1993, respectively.

Her internships included Fermilab, U.S. Naval Research Laboratory, and Cray Research. In 1993, she joined the Electrical and Computer Engineering Department, University of Colorado, Boulder, in 1993, where she is currently an Assistant Professor, overseeing an active research program in computational electromagnetics. Her work includes the development of methods to extract information from numerical simulations, and development of higher order techniques to reduce phase error in FDTD simulations. Her research is industrial-based with applications in high-speed analog and digital design, EMC/EMI, solar cell design, and wireless communications. She is also very active in engineering education, focusing on moving toward an interactive environment where the student is in charge of his or her learning. In this area, she is working on undergraduate engineering design issues and incorporating research into the classroom in an interactive and meaningful way. She is currently advising a National Science Foundation (NSF) Post-Doctoral Fellow in engineering education.

Prof. Piket-May received a 1996 URSI Young Scientist Award and was named a Sloan New Faculty Fellow in 1997. That same year, she also received an NSF CAREER Award for her research and teaching activities, and was elected to the Ad Com of the IEEE Antennas and Propagation Society.

Vythialingam Sathiaseelan is an Assistant Professor of Radiology at Northwestern University Medical School and Northwestern Memorial Hospital, Chicago, IL. He is an Associate Member of the Cancer Center, Northwestern University, and is a member of many professional organizations. His main research focuses on the development of improved EM techniques for heating deep-seated and superficial tumors and numerical modeling of EM interaction with biological objects.

Dr. Sathiaseelan is board certified in Therapeutic Radiological Physics by the American Board of Radiology.

Bharat B. Mittal is Professor of Radiology and Chief of Radiation Oncology at Northwestern University Medical School and Northwestern Memorial Hospital, Chicago, IL. He is also a member of the Cancer Center, Northwestern University, and a member of many professional organizations. His research involves management of head and neck cancers, lymphoid malignancies, and the use of hyperthermia with irradiation and/or chemotherapy in the treatment of a variety of malignant tumors.

Dr. Mittal is board certified by the American Board of Radiology.